Electron Affinities, Ionization Energies, and Fragmentation Energies of Fe_n Clusters ($n = 2-6$): A Density Functional Theory Study

Gennady L. Gutsev*,† and Charles W. Bauschlicher, Jr.‡

NASA Ames Research Center, Moffett Field, California 94035

Received: February 28, 2003; In Final Form: May 30, 2003

The electronic and geometrical structures of the ground and exited states of Fe_n, Fe_n^-, and Fe_n^+ are computed by density functional theory. Because the assignment of the ground states of Fe_3, Fe_3^-, Fe_4, and Fe_4^- is controversial, these systems are studied using several different functionals. It appears that the LSDA and B3LYP methods do not work well for iron clusters and should be avoided. The number of unpaired electrons in the neutral ground states is 6(Fe_2), 10(Fe_3), 14(Fe_4), 16(Fe_5), and 20(Fe_6). The number of unpaired electrons in the ground states of the anions and cations differ by one from the corresponding neutral, except for Fe_4^+, which has three fewer unpaired electrons than Fe_4. The computed DFT adiabatic electron affinities and ionization potentials of the neutral clusters are in good agreement with experiment. Fragmentation energies are in qualitative agreement with experiment, where the error is about 1 eV for the dissociation energy of the iron dimer. The natural bond analysis allows one to qualitatively understand the nature of high local magnetic moments at iron sites and their evolution from Fe_2 to Fe_6.

Introduction

Iron clusters have been found to act as catalysts for producing single-walled[1,2] carbon nanotubes (SWNT), which are expected to possess unique mechanical, electronic, magnetic, and optical properties. Smalley with co-workers[3] have developed a high-pressure high-temperature process where $Fe(CO)_5$ decomposes and forms iron clusters.[4] The latter catalyze the growth of SWNTs in the presence of a CO flow. Chemical vapor deposition techniques use CO or hydrocarbon feedstock and iron particles as a catalysist.[5] When CO is used as a feedstock, by analogy[6] with the Boudouard disproportionation reaction of producing atomic carbon from vibrationally excited carbon monoxide $CO(v) + CO(w) \rightarrow C + CO_2$, the critical step in the SWNT growth is believed to be due to $M-CO + CO \rightarrow M-C + CO_2$ (where M is a catalyst cluster) reactions. However, the mechanism of iron-catalyzed growth of SWNTs is not well understood;[7,8] for example, the size and the charge of the catalytic metal particles are unknown.

Experimental spectroscopic data for iron clusters are rather scarce. The bond length appears to be measured only for Fe_2 trapped in argon ($r_e = 1.87 \pm 0.13$ Å)[9] and neon ($r_e = 2.02 \pm 0.02$ Å)[10] matrixes. Vibrational frequencies were obtained for Fe_2 (299.6 cm^{-1}),[11] Fe_2^- (250 ± 20 cm^{-1}),[12] and Fe_3.[13,14] Nour et al.[13] assigned a band at 180 cm^{-1} to the Fe_3 ν_3 antisymmetric stretching frequency, but a recent resonance Raman spectroscopy study by Moscovits with co-workers[14] found that assignment of frequencies of Fe_3 is not straightforward "since the molecule does not have conventional asymmetric stretching and bending modes".

Electron affinities for clusters Fe_n up to $n = 34$ were measured[15,16] using photoelectron spectroscopy while ionization energies of the clusters up to $n = 100$ were obtained[17−19] using photoionization. Fragmentation energies of the Fe_n^+ clusters up to $n = 19$ were obtained[20−24] using collision-induced dissociation (CID) of the clusters with xenon. Bond dissociation $Fe_{n-1} + Fe$ energies of the neutral clusters were derived from the experimental values of ionization energies of the neutrals and fragmentation data for the corresponding cations.[25] Magnetic behavior of iron clusters is rather complicated.[26] A slow oscillating convergence of magnetic moments of Fe_n in the range of $25 \leq n \leq 700$ to the bulk value of 2.15 μ_B per atom has been observed in Stern-Gerlach deflection experiments.[27] The magnetic moment per atom for small iron clusters is larger (2.7−3.3 μ_B)[27,28] than those found for larger clusters or the bulk.

The ground state of Fe_2 has been the subject[29] of a great number of computations performed at different ab initio and density functional theory (DFT) levels. For larger clusters, we are aware of one ab initio study[30] based on configuration interaction (CI) single-point calculations at assumed or Hartree−Fock geometries. The spin multiplicities obtained in this study increase with the addition of each Fe atom by four from 7(Fe_2) to 23(Fe_6). The remaining computations[31−46] on iron clusters up to $n = 19$ have been performed mainly using the local spin density approximation (LSDA) often combined with the use of effective core potentials (ECP). Beyond the LSDA, Salahub et al.[34] used LSDA with so-called nonlocal gradient corrections (LSDA-NL) for the neutral, anionic, and cationic iron clusters up to $n = 5$. The number of unpaired electrons, $2S$ (where S is the net spin), was found[34,36,37] to be 6(Fe_2), 8(Fe_3), 12(Fe_4), 16-(Fe_5), and 20(Fe_6). This is in disagreement with the more recent DFT with a generalized gradient approximation for the exchange-correlation potential (DFT-GGA) computations,[32,40] which have predicted 10 unpaired electrons for Fe_3 and 14 for Fe_4. Using a Discrete Variational X_α method, Cheng and Ellis obtained[33] an even larger $2S$ value of 16 for Fe_4.

The most recent paper of Salahub and Chrétien,[47] published while the present work was in preparation, reported the results of calculations of Fe_n, Fe_n^-, and Fe_n^+ ($n = 1-4$) using DFT-GGA methods. They also obtained 10 and 14 unpaired electrons for Fe_3 and for Fe_4, respectively. For Fe_3^- and Fe_4 they found

* Corresponding author. E-mail: ggutsev@mail.arc.nasa.gov.
† ELORET Corp., Mail Stop 230−3.
‡ Space Technology Division, Mail Stop 230-3.

10.1021/jp030288p CCC: $25.00
Published on Web 08/14/2003

the ground states to be $^{12}B_1$ and $^{15}A''$, respectively, which is in agreement with the previous DFT-GGA work.[40,42] However, for Fe_3 they found an $^{11}A_2$ ground state, and an $^{11}A_1$ state, which previously[40] was assigned as the ground state, was found to be a transition state.

The purpose of this work is to determine the ground states and their geometrical structures of small Fe clusters, namely Fe_n, Fe_n^-, and Fe_n^+ ($n = 2-6$). We also report their vibrational frequencies and infrared intensities, as this may aid in the interpretation of future experimental work. Because this work will act as a building block for future studies of the chemistry of Fe clusters, it is important to calibrate our calculations against experiment, which consists mainly of the electron affinities, ionization energies, and fragmentation energies. While our main interest is the electronic and geometric structure of these clusters, previous work has shown some variation in results with choice of function, and therefore, we test the performance of several DFT-GGA approaches to establish the functional of choice for this class of systems.

Computational Details

We performed density-functional theory[48] calculations using several different functionals. Our primary exchange-correlation functional consisted of the combination of Becke's exchange[49] and Perdew-Wang's correlation functionals,[50] referred to as BPW91. For Fe_3 and Fe_4, several additional functionals are used, namely LSDA (Slater's exchange[51] and Vosko-Wilk-Nusair's correlation[52]), hybrid B3LYP,[53,54] BLYP (Becke's exchange[49] and Lee−Yang−Parr's correlation[55]), BP86 (Becke's exchange[49] and Perdew's correlation[56]), BPBE (Becke's exchange[49] and Perdew-Burke-Ernzerhof's correlation[57]), and PBEPBE (Perdew-Burke-Ernzerhof's exchange and correlation[57]).

The Gaussian 98 program[58] was used for all calculations. The 6-311+G* (15s11p6d1f)/[10s7p4d1f] basis set[59−61] was used. Calibration computations[62] were performed for Fe_2 with the recently developed[63] triple-ζ (TZ) correlation consistent basis set. The results obtained using the larger TZ basis set for the Fe_2 ground $^7\Delta_u$ state ($r_e = 2.00$ Å and $\omega_e = 404$ cm^{-1}) are only marginally different from those obtained with the 6-311+G* basis ($r_e = 2.01$ Å and $\omega_e = 397$ cm^{-1}). Thus, we conclude that expanding the basis set will not significantly affect the results. However, as we discuss below, the results depend somewhat on the choice of functional.

The geometry of each species was optimized for each possible spin multiplicity until further increasing the spin multiplicity would result in a state whose total energy is above the energy of the lowest asymptote. Subsequent frequency calculations were performed using analytical second derivatives to confirm that the optimized geometries correspond to minima. Our reported electron affinities and ionization energies correspond to adiabatic values, that is, they are computed as differences in total energies of the corresponding species, each at its equilibrium geometry. The values are corrected for the zero point energies (ZPEs), where the ZPEs are computed as one-half the sum of the vibrational frequencies. Fragmentation energies are also corrected for the ZPEs. To gain insight into the nature of chemical bonding in iron clusters, we have performed Natural Bond orbital Analysis.[64,65]

Results and Discussion

Iron Dimer. The ground state of iron atom is ^5D and corresponds to a $4s^23d^6$ occupation. In the Fe_2 dimer, one or two 4s electrons are promoted into the 3d-manifold. If one 4s electron is promoted, then so-called mixed states are formed

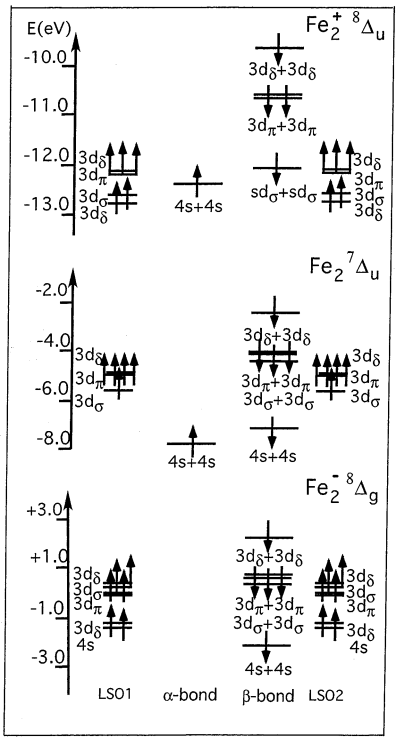

Figure 1. Bonding patterns of ground-state Fe_2, Fe_2^-, and Fe_2^+.

(the asymptote is $4s^23d^6 + 4s^13d^7$). The lowest mixed state is $^9\Sigma_g^-$, which is found to be the ground state in recent[66,67] multireference CI (MRCI) calculations. If both 4s electrons are promoted (the asymptote is $4s^13d^7 + 4s^13d^7$), the lowest state is $^7\Delta_u$, which is identified as the ground state in DFT studies[29] and some ab initio methods.[30] The difference between these two states is best seen by using the NBO analysis. This analysis operates with localized (Lewis) bonding orbitals, which appear to be well suited for describing the chemical bonding of the 3d metal dimers. The NBO orbitals can be identified as bonding (4s + 4s), ($3d_\sigma + 3d_\sigma$) (or hybridized ($3d_\sigma 4s + 3d_\sigma 4s$)), ($3d_\pi + 3d_\pi$), and ($3d_\delta + 3d_\delta$) or as the corresponding antibonding orbitals in each spin representation. Note that occupation of a bonding−antibonding pair of the same type results in two localized spin−orbitals (LSO) of a pure atomic character.[68]

The bonding pattern[69] of the $^7\Delta_u$ ($4s^13d^7 + 4s^13d^7$) state is presented in Figure 1. As can be seen, the 4s electrons occupy a two-electron (4s + 4s) bond, while the four spin down 3d electrons fill the four lowest-energy bonding orbitals. Ten spin-up 3d electrons are chemically inactive and occupy the LSOs. The bottom panel of Figure 1 presents the bonding pattern of the ground $^8\Delta_g$ state of Fe_2^-. An extra electron attaches to the spin-up 4s−4s antibonding orbital of Fe_2 that destroys the spin up 4s + 4s bond and creates two 4s LSOs, while the spin-down part of the 4s + 4s bond remains the same. The bonding pattern in the mixed $^9\Sigma_g^-$ state of Fe_2 is the same as $^8\Delta_g$ state of Fe_2^-, except ($3d_\delta + 3d_\delta$) orbital is empty in the $^9\Sigma_g^-$ state.

At the DFT level, the additional 0.87 eV 4s→3d promotion energy[70] for the $^7\Delta_u$ state has been compensated for by the energy gained due to the formation of two one-electron bonds in the $^7\Delta_u$ state with respect to those in the $^9\Sigma_g^-$ state. While the BPW91 favors the bond formation and places $^7\Delta_u$ below $^9\Sigma_g^-$ by 0.51 eV (similar values were obtained using other functionals, see Table 1), the MRCI methods predict[66,67] opposite order for these two states.

In the ground $^8\Delta_u$ state of Fe_2^+, the electron formally leaves the (4s+4s) bonding orbital of Fe_2. However, the nearly pure

TABLE 1: Different States of Fe_2, Fe_2^-, and Fe_2^+ Computed at the BPW91 and PP86 Levels[a]

	BPW91			PP86[b]		
state	ΔE, eV	r_e, Å	ω_e, cm^{-1}	ΔE, eV	r_e, Å	ω_e, cm^{-1}
			Fe_2			
$^7\Delta_u$	0.00	2.011	397	0.00	2.008	415
$^9\Delta_g$	+0.48	2.256	279			
$^9\Sigma_g^-$	+0.51	2.152	331	+0.53	2.151	332
$^7\Delta_g$	+0.65	2.103	366			
$^9\Delta_u$	+0.84	2.356	256			
$^5\Sigma_g^-$	+0.84	1.834	476	+0.84	1.860	510
			Fe_2^-			
$^8\Delta_g$	−0.94	2.071	351	−1.17	2.073	358
$^6\Delta_g$	−0.53	2.051	361	−0.84	2.050	370
$^8\Delta_u$	−0.34	2.174	315			
$^6\Sigma_u^-$	−0.09	1.879	423			
			Fe_2^+			
$^8\Delta_u$	+6.68	2.172	319	+7.14	2.180	319
$^8\Delta_g$	+7.08	2.264	290	+7.50	2.271	296
$^6\Delta_g$	+7.95	1.946	416	+7.94	1.949	454
$^6\Delta_u$	+7.96	2.081	350			
$^{10}\Sigma_g^-$	+8.00	2.360	243	+8.51	2.373	240

[a] Total energy shifts (ΔE) are given with respect to the ground state of Fe_2. Experiment: Fe_2, $r_e = 2.02 \pm 0.02$ Å,[10] $\omega_e = 299.6$ cm^{-1};[11] Fe_2^-, $\omega_e = 250 \pm 20$ cm^{-1} (ref 12). [b] Ref. 47.

($3d_\sigma + 3d_\sigma$) orbital of Fe_2 becomes a strongly mixed ($3d_\sigma 4s + 3d_\sigma 4s$) orbital in Fe_2^+, see Figure 1.

Table 1 presents the spectroscopic constants of the ground and some excited states of Fe_2, Fe_2^-, and Fe_2^+. They are compared to those obtained recently by Salahub and Chrétien[47] at the PP86 level. The available experimental results for the ground states of Fe_2 and Fe_2^- are in reasonable agreement with the theory, although the differences in vibrational frequencies appear to be rather large. This is somewhat puzzling, since the Fe−Fe frequency computed for Fe_2CO at the BPW91/6-311+G* level is in much better agreement with experiment[71] (the difference is about 40 cm^{-1}). The same behavior is observed for the Co−Co frequencies in Co_2 and Co_2CO; while the BPW91 frequency[68] of Co_2 is about 100 cm^{-1} higher than the experimental value, the discrepancy[72] is reduced to 11 cm^{-1} in Co_2CO.

Ground State of the Iron Trimer. The first DFT-GGA study[40] predicted an $^{11}A_1$ ground state of Fe_3, while the more recent work of Salahub and Chrétien[47] predicts an $^{11}A_2$ ground state and that the $^{11}A_1$ state is not even a minimum. Therefore, we first study these two states, as well as the lowest $^{11}B_1$ and $^{11}B_2$ states, in detail. To answer if the ground state depends on the choice of functional, we study these four states using several functionals. In additional to the variation with functional, we compute the frequencies with the standard (the integration grid is FINE) and tight (Opt=TIGHT, Grid=UltraFINE) options, because it is known[73] that molecular properties, especially vibrational frequency, may strongly be influenced by the accuracy of the integration.

At all levels of theory used, the $^{11}A_1$ and $^{11}A_2$ states are nearly degenerate in total energy. For all of the functionals used in this work, the $^{11}A_1$ is a minimum, which contradicts the result of Salahub and Chrétien,[47] who found the $^{11}A_1$ to be a transition state. The $^{11}A_2$ state is a minimum for all functionals, except BLYP. As shown in Table 2, the $^{11}A_2$ state is the ground state at the BPW91, BP86, BPBE, and PP86 levels. The PBEPBE approach predicts the $^{11}A_2$ state to be degenerate in total energy with the $^{11}A_1$ state (see Table 3) and places the $^{11}A_1$ state slightly below (by 0.004 eV) if the tight option is used. The BLYP level predicts the $^{11}A_2$ state to be a transition state. Note that the choice of grid affects the lowest frequency which decreases with respect to that computed using the standard (FINE) integration option. The largest computed separation between the $^{11}A_2$ and $^{11}A_1$ states is +0.012 eV, which is obtained at the BPBE level. Because such a small difference is beyond the accuracy of the current computations, one may conclude that higher levels of theory are required for an assignment of $^{11}A_1$ or $^{11}A_2$ as the ground state of Fe_3.

Table 4 shows that the $^{11}B_2$ state is above the $^{11}A_2$ state by 0.17−0.19 eV. Again, only the BLYP level predicts this state to be a transition state. The BLYP predicts the $^{11}B_1$ state to be a minimum, while the BPW91 and BPBE predict this state to be a transition state in computations performed with the standard grid. The BP86 and PBEPBE levels require a tighter integration to arrive at the same conclusion. The PP86 level produces the bond lengths and vibrational frequencies, which are close to those obtained at the BLYP level, and also predicts the $^{11}B_1$ state to be a minimum. While four levels, BPW91, BP86, BPBE, and PBEPBE, provide similar results, the BPW91 frequencies appear to be less sensitive to the integration quality. In addition to the differences in functionals used, our results suggest that some of the disagreement between our results and those of Salahub and Chrétien[47] may be due to the grid used. We should also note that some differences could arise from their computation of the vibrational frequencies by finite differences compared with our use of analytical second derivatives.

Note that all three stable states found have the $Fe_2Fe_1Fe_3$ angle less than 60°, which is expected to enhance the bonding between

TABLE 2: $^{11}A_2$ State of Fe_3 Computed Using the BPW91, BLYP, BP86, BPBE, PBEPBE (Using Two Sample Grids for Integrating Exchange-Correlation Energy Contribution), and PP86 Levels[a]

method	ΔE_{tot} eV	$R_{1,2;1,3}$ Å	$R_{2,3}$ Å	∠213°	$\omega(b_2)cm^{-1}$	$\omega(a_1)$ cm^{-1}	$\omega(a_1)$ cm^{-1}
			$^{11}A_2$ (α: a_1-a_2-b_1-b_2 || β: a_1-a_2-b_1-b_2) (19−5−7−13 || 15−3−6−10) Grid = **FINE**			
BPW91	0.0	2.303	2.166	56.1	56	232	354
BLYP	+0.004	2.324	2.188	56.2	58i	227	341
BP86	0.0	2.296	2.162	56.2	29	234	357
BPBE	0.0	2.300	2.165	56.1	60	233	355
PBEPBE	0.0	2.301	2.171	56.3	31	234	352
PP86	0.0	2.313	2.176	56.1	56	235	347
			$^{11}A_2$ (19−5−7−13 || 15−3−6−10) Grid = **UltraFINE**				
BPW91	0.0	2.301	2.167	56.1	48	231	352
BLYP	+0.003	2.323	2.189	56.2	68i	225	339
BP86	0.0	2.295	2.164	56.2	7	233	354
BPBE	0.0	2.300	2.166	56.1	53	231	352
PBEPBE	+0.004	2.300	2.172	56.3	15	233	350

[a] The PP86 results are from ref 47. Total energy shifts (ΔE) are given with respect to the lowest energy state obtained by the corresponding method and grid.

TABLE 3: $^{11}A_1$ State of Fe_3 Computed Using the BPW91, BLYP, BP86, BPBE, PBEPBE (Using Two Sample Grids for Integrating Exchange-Correlation Energy Contribution), and PP86 Levels[a]

method	ΔE_{tot} eV	$R_{1,2;1,3}$ Å	$R_{2,3}$ Å	∠213°	$\omega(b_2)cm^{-1}$	$\omega(a_1)$ cm^{-1}	$\omega(a_1)$ cm^{-1}
			$^{11}A_1$ (19−5−7−13 || 16−2−6−10) Grid = **FINE**				
BPW91	+0.011	2.330	2.095	53.4	75	249	365
BLYP	0.0	2.350	2.117	53.5	33	242	355
BP86	+0.002	2.323	2.091	53.5	66	251	367
BPBE	+0.012	2.328	2.093	53.4	76	250	365
PBEPBE	0.0	2.328	2.099	53.6	65	252	364
PP86	0.077	2.339	2.103	53.4	54i	253	357
			$^{11}A_1$ (19−5−7−13 || 16−2−6−10) Grid = **UltraFINE**				
BPW91	+0.011	2.329	2.094	53.4	70	247	365
BLYP	0.0	2.350	2.117	53.5	16	239	353
BP86	+0.001	2.322	2.090	53.5	61	249	368
BPBE	+0.010	2.328	2.093	53.4	71	248	366
PBEPBE	0.0	2.327	2.099	53.6	60	250	364

[a] The PP86 results are from ref 47. Total energy shifts (ΔE) are given with respect to the lowest energy state obtained by the corresponding method and grid.

TABLE 4: $^{11}B_2$ State of Fe_3 Computed Using the BPW91, BLYP, BP86, BPBE, PBEPBE (Using Two Sample Grids for Integrating Exchange-Correlation Energy Contribution), and PP86 Levels[a]

method	ΔE_{tot} eV	$R_{1,2;1,3}$ Å	$R_{2,3}$ Å	∠213°	$\omega(b_2)cm^{-1}$	$\omega(a_1)$ cm^{-1}	$\omega(a_1)$ cm^{-1}
			$^{11}B_2$ (19−5−7−13 || 16−3−5−10) Grid = **FINE**				
BPW91	+0.19	2.259	2.225	59.0	193	347	1713
BLYP	+0.16	2.279	2.247	59.1	1470i	187	334
BP86	+0.18	2.251	2.222	59.1	195	350	1651
BPBE	+0.18	2.256	2.224	59.1	194	347	1509
PBEPBE	+0.17	2.256	2.231	59.3	199	346	1255
PP86	+0.22	2.254	2.251	59.9	Not Computed		
			$^{11}B_2$ (19−5−7−13 || 16−3−5−10) Grid = **UltraFINE**				
BPW91	+0.19	2.258	2.226	59.0	197	349	1527
BLYP	+0.16	2.281	2.244	58.9	995i	190	337
BP86	+0.18	2.250	2.224	59.1	199	352	1265
BPBE	+0.19	2.256	2.225	59.1	198	350	1379
PBEPBE	+0.17	2.255	2.232	59.3	204	349	1096

[a] The PP86 results are from ref 47. Total energy shifts (ΔE) are given with respect to the lowest energy state obtained by the corresponding method and grid.

TABLE 5: $^{11}B_1$ State of Fe_3 Computed Using the BPW91, BLYP, BP86, BPBE, PBEPBE (Using Two Sample Grids for Integrating Exchange-Correlation Energy Contribution), and PP86 Levels[a]

method	ΔE_{tot} eV	$R_{1,2;1,3}$ Å	$R_{2,3}$ Å	∠213°	$\omega(b_2)cm^{-1}$	$\omega(a_1)$ cm^{-1}	$\omega(a_1)$ cm^{-1}
			$^{11}B_1$ (18−5−7−14 || 15−3−6−10) Grid = **FINE**				
BPW91	+0.001	2.208	2.353	64.4	50i	199	353
BLYP	+0.002	2.229	2.377	64.4	74	191	339
BP86	0.000	2.203	2.347	64.4	36	200	357
BPBE	0.000	2.207	2.349	64.3	57i	200	355
PBEPBE	0.000	2.211	2.353	64.3	32	201	352
PP86	+0.004	2.219	2.363	64.3	73	198	345
			$^{11}B_1$ (18−5−7−14 || 15−3−6−10) Grid = **UltraFINE**				
BPW91	+0.001	2.210	2.353	64.4	63i	197	350
BLYP	+0.001	2.229	2.380	64.4	80	189	338
BP86	0.000	2.204	2.346	64.4	20i	198	353
BPBE	0.002	2.208	2.350	64.3	69i	198	351
PBEPBE	0.004	2.212	2.352	64.3	22i	199	349

[a] The PP86 results are from ref 47. Total energy shifts (ΔE) are given with respect to the lowest energy state obtained by the corresponding method and grid.

Fe_2 and Fe_3. Unlike Salahub and Chrétien,[47] we found all the states with the $Fe_2Fe_1Fe_3$ angles larger than 60°, including the $^{11}B_1$ state given in Table 5, to be transition states.

Comparison of Performance of LSDA, B3LYP, and DFT-GGA Levels. Because there are rather accurate experimental data for the EAs of iron clusters,[15,16] it is interesting to compare the performance of different methods for Fe_3 and Fe_4, where the LSDA and DFT-GGA levels predict the ground states of different net spins. Computations were performed using the LSDA, B3LYP, BLYP, BP86, BPBE, PBEPBE, and BPW91 levels for the A′ and A″ states of Fe_3 and Fe_3^- for 2S values of 8 and 10 for the neutral and 9 and 11 for the anion. (Because some of the functionals yield C_s symmetry, all of the results are given in this symmetry, even though most functionals yield C_{2v} symmetry). Computations on Fe_4 and Fe_4^- are performed without any symmetry constraints for 2S values of 12 and 14 for the neutral and 13 and 15 for the anion. The initial guess orbitals in each optimization were taken from the corresponding BPW91 calculation. The results of calculations are presented in Tables 6−9 (frequencies and dipole moments) and Figures 2−5 (geometries and Mulliken atomic charges and open-shell occupation per atom in the anions and cations). The open-shell occupation is consistent with experimental measurements of local magnetic moments on atoms, because the magnetic

TABLE 6: Vibrational Frequencies, Dipole Moments, and Relative Total Energies of Two Candidates for the Ground State of Fe_3 Computed at Different Levels

Fe_3 (2S+1 = 9)

	LSDA	B3LYP	BLYP	BP86	BPBE	PBEPBE	BPW91
	$^9A''$	$^9A''$	$^9A''$	$^9A''$	$^9A''$	$^9A''$	$^9A''$
ω_1, cm^{-1}	255	227	218	219	222	227	222
ω_2	255	229	218	221	224	228	223
ω_3	412	360	363	378	375	373	374
μ, Debye	0.00	0.00	0.00	0.00	0.00	0.00	0.00
ΔE_{tot}, eV	0.0	+1.25	+0.13	+0.17	+0.25	+0.22	+0.25

Fe_3 (2S+1 = 11)

	LSDA	B3LYP	BLYP	BP86	BPBE	PBEPBE	BPW91
	$^{11}A'$	$^{11}A'$	$^{11}A'$	$^{11}A''$	$^{11}A''$	$^{11}A''$	$^{11}A''$
ω_1, cm^{-1}	66	95	51	85	49	32	62
ω_2	221	150	207	232	231	234	231
ω_3	393	210	347	355	353	352	353
μ, Debye	0.47	0.61	0.56	0.74	0.78	0.75	0.78
ΔE_{tot}, eV	+0.22	0.0	0.0	0.0	0.0	0.0	0.0

TABLE 7: Vibrational Frequencies and Total Energy Shift Relative to Those of the Corresponding Neutral Ground States of Fe_3^- Computed at Different Levels[a]

Fe_3^- (2S+1 = 10)

	LSDA	B3LYP	BLYP	BP86	BPBE	PBEPBE	BPW91
	$^{10}A''$	$^{10}A''$	$^{10}A''$	$^{10}A''$	$^{10}A''$	$^{10}A''$	$^{10}A''$
ω_1, cm^{-1}	240	104	145	187	156	171	175
ω_2	250	145	174	206	179	183	178
ω_3	372	208	305	258	319	318	318
ΔE_{tot}, eV	−1.52	−0.88	−0.84	−1.02	−0.82	−0.87	−0.80

Fe_3^- (2S+1 = 12)

	LSDA	B3LYP	BLYP	BP86	BPBE	PBEPBE	BPW91
	$^{12}A'$	$^{12}A''$	$^{12}A''$	$^{12}A''$	$^{12}A''$	$^{12}A''$	$^{12}A''$
ω_1, cm^{-1}	22	112	206	188	212	213	211
ω_2	274	155	207	206	213	215	212
ω_3	370	199	307	258	322	320	321
ΔE_{tot}, eV	**−1.69**	**−1.33**	**−1.32**	**−1.61**	**−1.46**	**−1.48**	**−1.47**

[a] The bold-font values correspond to the experimental EA of 1.43(6) taken with the opposite sign.

TABLE 8: Comparison of Vibrational Frequencies, Dipole Moments, and Relative Total Energy Shifts of Two Candidates for the Ground State of Fe_4 Computed at Different Levels

Fe_4 (2S+1 = 13) C_1

	LSDA	B3LYP	BLYP	BP86	BPBE	PBEPBE	BPW91
ω_1, cm^{-1}	181	43	146	153	152	155	152
ω_2	193	100	156	162	161	165	161
ω_3	196	136	168	184	186	185	186
ω_4	196	160	168	185	187	185	187
ω_5	306	199	265	279	278	279	278
ω_6	409	269	358	373	370	369	371
μ, Debye	0.00	1.05	0.00	0.00	0.00	0.00	0.00
ΔE_{tot}, eV	0.0	+0.50	0.00	+0.02	+0.09	+0.06	+0.08

Fe_4 (2S+1 = 15) C_1

	LSDA	B3LYP	BLYP	BP86	BPBE	PBEPBE	BPW91
ω_1, cm^{-1}	128	119	93	104	105	106	104
ω_2	141	128	113	125	125	128	125
ω_3	256	151	202	207	201	208	200
ω_4	261	164	202	207	201	208	201
ω_5	262	215	220	230	229	231	228
ω_6	394	266	332	351	347	347	347
μ, Debye	0.00	0.05	0.00	0.00	0.00	0.00	0.00
ΔE_{tot}, eV	+0.30	0.0	0.0	0.0	0.0	0.0	0.0

moment is $\mu = g\mu_B S$ within the Heisenberg model (where g is close to 2.0, μ_B is Bohr magneton, and **S** is the spin operator). That is, the open-shell occupation is essentially gS.

As seen in Table 6, all methods predict the lowest state of Fe_3 with 2S = 8 to be A″, while there is a competition between the A′ and A″ states for 2S = 10. Only the LSDA level predicts $^9A''$ as the lowest state; the geometry of this state is an equilateral triangle at all levels of theory. The B3LYP level has placed the $^9A''$ state too high with respect to the $^{11}A'$ state. At the LSDA, B3LYP, and BLYP levels, the $^{11}A'$ state is below the $^{11}A''$ state, while the remaining methods predict the $^{11}A''$ state to be the more stable of the two. As shown in Figure 2, the $^{11}A''$ state is an isosceles triangle with the $Fe_2Fe_1Fe_3$ angle smaller than 60°, while the $^{11}A'$ state has an angle larger than

TABLE 9: Comparison of Vibrational Frequencies and Total Ergies with Respect to Those of the Corresponding Ground State Neutrals of Fe_4^- Computed at Different Levels[a]

Fe_4^- (2S+1 = 14) C_1

	LSDA	B3LYP	BLYP	BP86	BPBE	PBEPBE	BPW91
ω_1, cm^{-1}	176	52	137	144	141	147	141
ω_2	191	99	158	162	162	166	162
ω_3	221	142	191	200	177	203	199
ω_4	223	144	192	202	211	209	202
ω_5	244	188	197	212	229	217	210
ω_6	395	256	341	357	354	355	354
ΔE_{tot}, eV	**−2.00**	−1.11	−1.32	−1.58	−1.34	−1.41	−1.36

Fe_4^- (2S+1 = 16) C_1

	LSDA	B3LYP	BLYP	BP86	BPBE	PBEPBE	BPW91
ω_1, cm^{-1}	154	147	75	75	53	79	81
ω_2	181	181	102	93	99	82	82
ω_3	230	186	122	129	131	133	129
ω_4	264	187	176	184	185	187	183
ω_5	264	240	195	204	206	206	205
ω_6	381	296	324	340	340	340	340
ΔE_{tot}, eV	−1.97	**−1.81**	**−1.51**	**−1.88**	**−1.75**	**−1.77**	**−1.76**

[a] The bold-font values correspond to the experimental EA of 1.78(6) taken with the opposite sign.

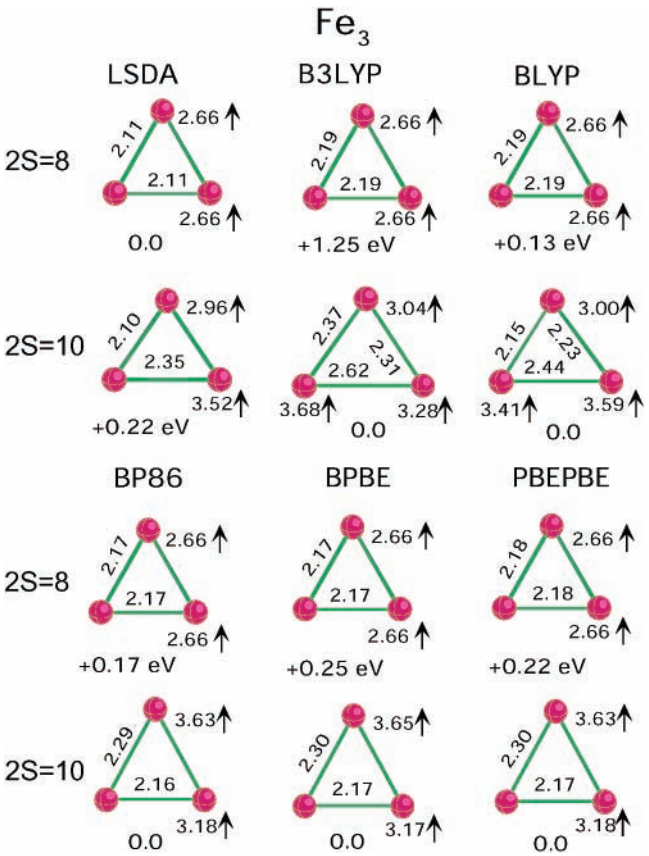

Figure 2. Bond lengths and Mulliken open-shell occupation per atom obtained for Fe_3 at different levels of theory.

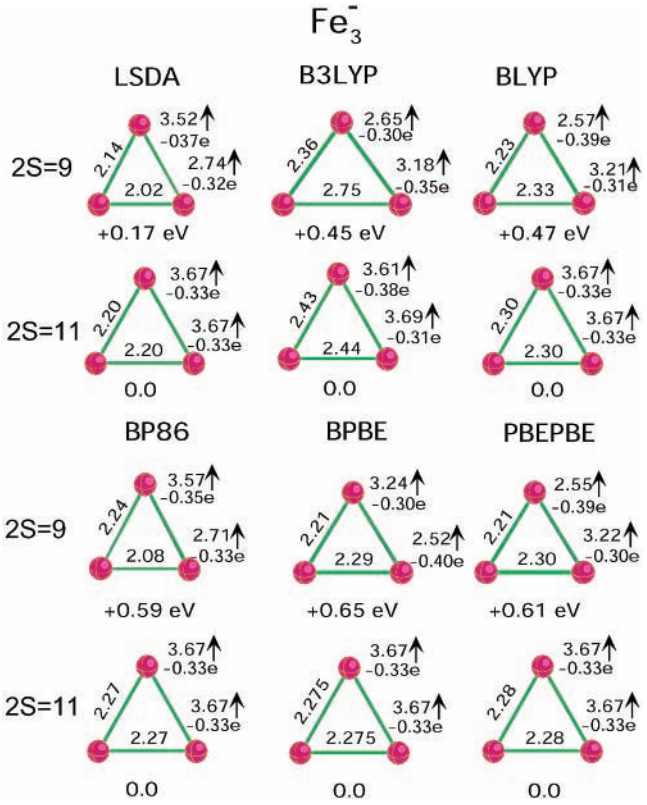

Figure 3. Bond lengths and Mulliken atomic charges and open-shell occupation per atom obtained for Fe_3^- at different levels of theory.

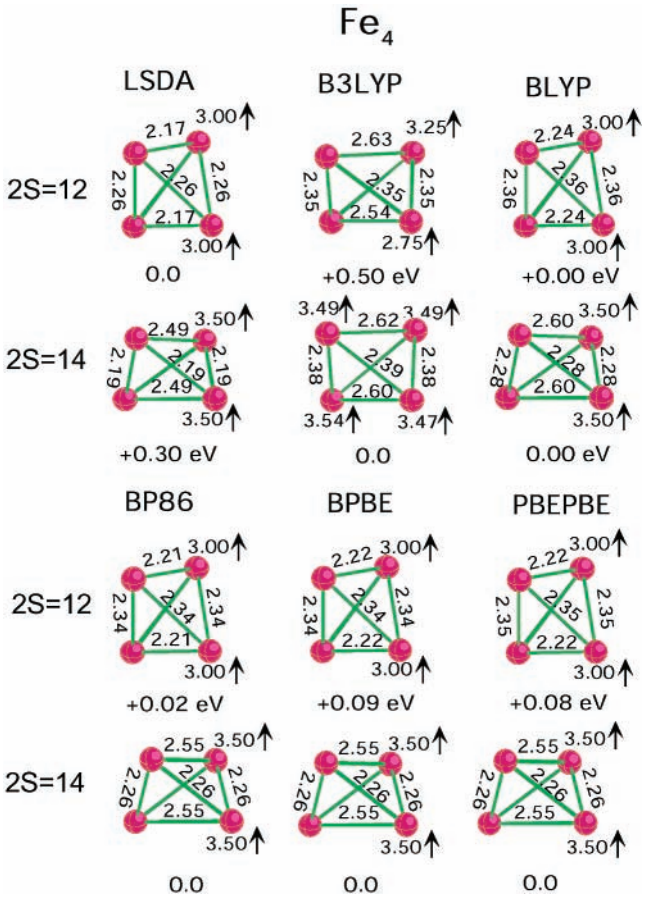

Figure 4. Bond lengths and Mulliken atomic charges and open-shell occupation per atom obtained for Fe_4 at different levels of theory.

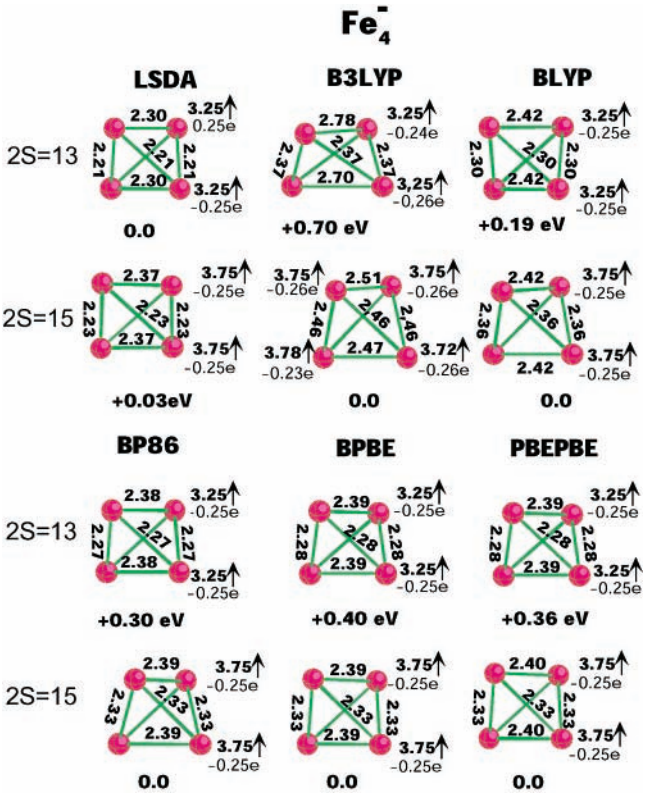

Figure 5. Bond lengths and Mulliken atomic charges and open-shell occupation per atom obtained for Fe_3^- at different levels of theory.

60°. It is interesting to note that the B3LYP and BLYP approaches predict a triangle with all bond lengths different.

The results of calculations on the Fe_3^- anion are less dependent on the choice of functional as shown in Table 7 and Figure 3. Excluding LSDA, all the levels yield a $^{10}A''$ ground state, which is appreciably below the $^{12}A''$ state; the LSDA predicts the ground state to be $^{12}A'$. The geometry of the $^{12}A''$ state ($^{12}A'$, LSDA) is an equilateral triangle. As shown in Table 7, the adiabatic electron affinities computed at all levels are in rather good agreement with experiment. The largest discrepancy of 0.25(6) eV is obtained at the LSDA level. The best values are obtained at the BPBE, PBEPBE, and BPW91 levels, where the difference with experiment does not exceed 0.05(6) eV.

As shown in Table 8 and Figure 4, the performance of the BLYP, BP86, BPBE, PBEPBE, and BPW91 levels for Fe_4 is rather similar. All of them predict similar geometries (of D_{2h} shape), vibrational frequencies, and place the state with 2S = 14 slightly below the state with 2S = 12. The B3LYP level predict distorted geometries and places the 2S = 12 state well above the 2S = 14 state. Only the LSDA predicts the 2S = 12 state as the ground state, as found in the previous LSDA studies.

A similar trend is found for the Fe_4^- anion (see Table 9 and Figure 5). The B3LYP predicts geometries of the 2S = 13 and 2S = 15 in large variance with those obtained at the rest of the levels. The LSDA seems to underestimate some bond lengths by as much as 0.1 Å and predicts the 2S = 13 state to be the lowest one. Again, the adiabatic electron affinities computed at all the levels are in good agreement with experiment. The largest deviations are obtained at the LSDA [+0.22(6) eV] and BLYP [-0.27(6) eV] levels. The EAs obtained at the BPBE, PBEPBE, and BPW91 levels are in excellent agreement with experimental values.

BPW91 Results on the Fe_n, Fe_n^-, and Fe_n^+ Clusters. As found in the previous section, the Perdew's correlation functionals yield very similar results that depend only marginally on the choice of the exchange functional (compare the BPBE

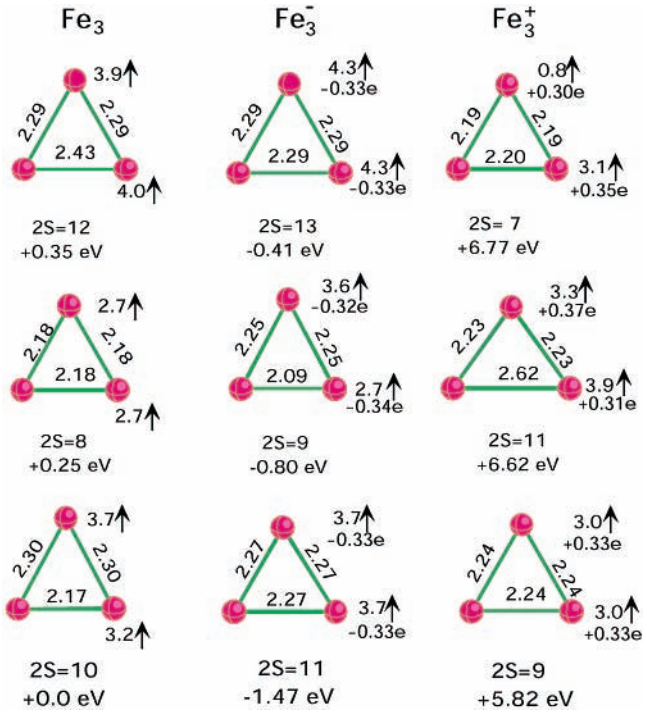

Figure 6. Bond lengths and Mulliken atomic charges and open-shell occupation per atom obtained for Fe_3, Fe_3^-, and Fe_3^+ obtained at the BPW91 level.

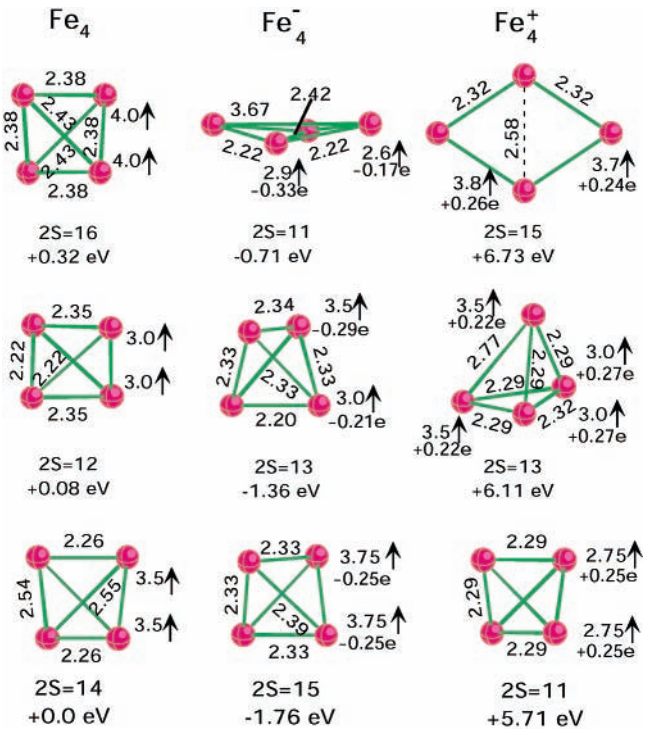

Figure 7. Bond lengths and Mulliken atomic charges and open-shell occupation per atom obtained for Fe_4, Fe_4^-, and Fe_4^+ obtained at the BPW91 level.

and PBEPBE results); therefore, the remaining computations were performed at the BPW91 level. Figures 6−9 show the geometries and Mulliken open-shell occupation per atom of the Fe_n, Fe_n^-, and Fe_n^+ clusters ($n = 3-6$), as well as the Mulliken atomic charges in charged clusters. The atomic charges in neutral clusters are nearly zero and not shown in the figures. Vibrational frequencies and relative IR intensities of the ground-state clusters are given in Table 10.

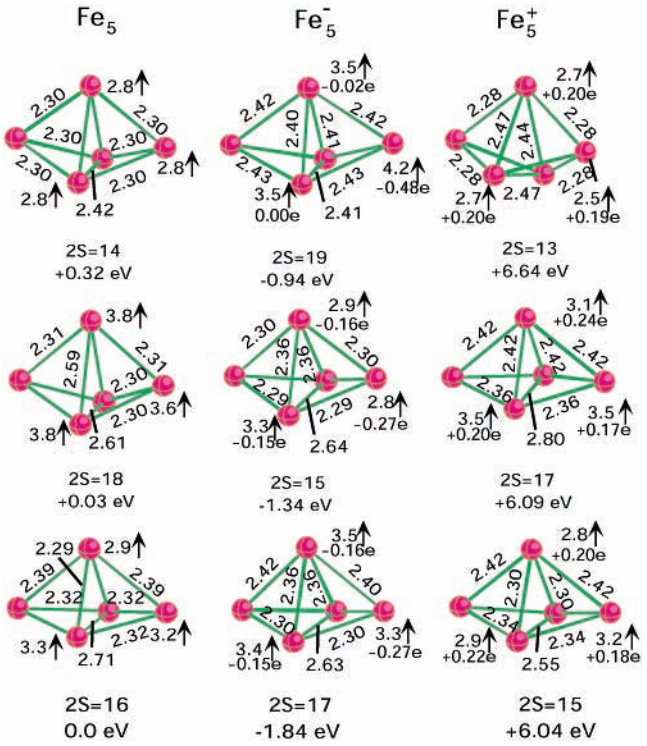

Figure 8. Bond lengths and Mulliken atomic charges and open-shell occupation per atom obtained for Fe_5, Fe_5^-, and Fe_5^+ obtained at the BPW91 level.

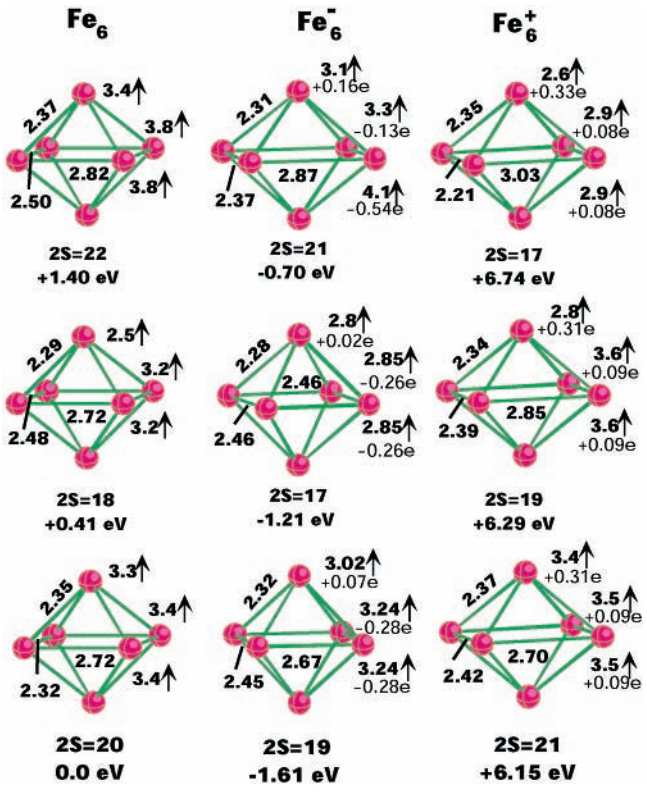

Figure 9. Bond lengths and Mulliken atomic charges and open-shell occupation per atom obtained for Fe_6, Fe_6^-, and Fe_6^+ obtained at the BPW91 level.

The ground state of Fe_3^+ has $2S = 9$; one less than the ground state of Fe_3, which is in agreement with a one-electron nature of electron detachment process. The same holds for Fe_2^+, Fe_5^+, and Fe_6^+, while Fe_4^+ is an exception, since its lowest energy state has $2S = 11$, in agreement with the previous theoretical

TABLE 10: Computed Vibrational Frequencies (cm^{-1}) and IR Relative Intensities (Arbitrary Units) of the Ground-State Fe_n, Fe_n^-, and Fe_n^+ Clusters[a]

	ω_1	ω_2	ω_3	ω_4	ω_5	ω_6	ω_7	ω_8	ω_9	ω_{10}	ω_{11}	ω_{12}
Fe_3	62 [1]	231 [0.05]	353 [0.00]									
Fe_3^-	214 [0.40]	214 [1]	325 [0.09]									
Fe_3^+	125 [0.25]	143 [1]	328 [0.56]									
Fe_4	104 [0.00]	125 [0.59]	200 [1]	201 [0.91]	228 [0.00]	345 [0.00]						
Fe_4^-	81 [0.99]	81 [1]	129 [0.00]	183 [0.00]	205 [0.00]	340 [0.00]						
Fe_4^+	153 [0.00]	155 [0.00]	245 [0.97]	247 [1]	247 [1]	372 [0.00]						
Fe_5	107 [0.02]	107 [0.01]	121 [1]	161 [0.53]	194 [0.00]	223 [0.55]	232 [0.07]	281 [0.03]	350 [0.17]			
Fe_5^-	80 [0.02]	90 [0.02]	148 [0.04]	166 [0.05]	202 [0.00]	221 [0.01]	244 [0.03]	279 [1]	337 [0.01]			
Fe_5^+	74 [0.02]	123 [0.02]	153 [0.37]	158 [0.04]	179 [0.00]	220 [0.47]	248 [1]	275 [0.18]	352 [0.02]			
Fe_6	53 [0.06]	116 [0.00]	148 [0.01]	151 [0.00]	163 [0.00]	175 [0.00]	205 [0.00]	235 [0.00]	245 [0.25]	256 [1]	301 [0.42]	337 [0.00]
Fe_6^-	86 [0.20]	99 [0.00]	144 [0.00]	148 [0.00]	173 [0.00]	180 [0.00]	202 [0.00]	207 [0.01]	257 [1]	265 [0.30]	295 [0.17]	336 [0.00]
Fe_6^+	65 [0.03]	105 [0.00]	150 [0.00]	152 [0.01]	177 [0.00]	197 [0.00]	212 [0.00]	216 [0.00]	233 [0.85]	259 [0.50]	269 [1]	320 [0.00]

[a] Absolute intensity ratios Neutral/Anion/Cation (each in km/mole); Fe_3, 36.44:0.02:1.86; Fe_4, 2.53:0.0012:3.31; Fe_5, 4.23:1.64:7.54; Fe_6, 3.09: 3.72: 3.94.

results.[34,47] No such violation of the "±1 rule" is found for the anions from Fe_2^- to Fe_6^-. As was noticed before, [37,47] the excited states of Fe_4 and its ions may have planar or near-planar geometrical configurations; we find planar structure for some excited states of the ions, see Figure 7.

As shown in Figure 8, the neutral and charged Fe_5 clusters in the ground and lowest excited states possess distorted D_{3h} geometries. The neutral ground state has $2S = 17$; a similar structure and the same net spin were found in the previous LSDA calculations.[34] However, the LSDA bond lengths[34] are shorter by ~0.1 Å with respect to those found at the DFT-GGA levels. No geometries were reported for either Fe_5^- or Fe_5^+. Attachment or detachment of an electron results in changes of the bond lengths up to 0.08 Å without changing the geometrical shape (see Figure 8). The charges are nearly evenly distributed in Fe_5^+, while two apex atoms of Fe_5^- have somewhat larger charges and smaller open-shell occupations.

The first ECP LSDA calculations[36] on the neutral Fe_6 cluster predicted a caped trigonal bipyramid. Subsequent LSDA calculations[37,41] predicted a compressed D_{2h} distorted octahedron with $2S = 20$ for the ground state of Fe_6. The latter is in agreement with our computations (see Figure 9). However, there is a large difference in the bond lengths: the LSDA predicts[41] the range of 2.29−2.53 Å, while the BPW91 provides the range of 2.32−2.72 Å. Attachment or detachment of an electron does not seriously affect the bond lengths in the corresponding ground-state Fe_6^- and Fe_6^+ ions. However, the charge distributions are different; in the anion, the charge is mostly localized on the rectangular base, while in the cation, it is localized on the apex atoms.

Vibrational Frequencies of the Fe_n, Fe_n^-, and Fe_n^+ Clusters. Harmonic vibrational frequencies computed for the ground state neutral and charged iron clusters are presented in Table 10. The frequencies are generally small; the smallest frequency of 53 cm^{-1} belongs to Fe_6, while the largest frequency of 372 cm^{-1} belongs to Fe_4^+. Many modes have rather small IR intensities. The modes of Fe_3^- and Fe_4^- possess especially low intensities (see footnote to Table 10).

The LSDA and DFT-GGA frequencies have been reported[34] for neutral Fe_n ($n = 2-5$). For Fe_2, the LSDA and DFT-GGA frequencies are 497 cm^{-1} and 474 cm^{-1}, respectively; for Fe_3, the frequencies are similar to our LSDA values for the $^9A''$ state given in Table 6 (the largest difference is less than 20 cm^{-1}), while the LSDA vibrational frequencies of Fe_4 are in a large variance with our LSDA frequencies presented in Table 8 for $2S = 12$ and are closer to those computed for $2S = 14$ (where the largest difference is 20 cm^{-1}).

Salahub and Chrétien[47] reported vibrational frequencies for the ground-state Fe_3, Fe_3^+, and Fe_4^+ clusters computed at the PP86 level. While our BPW91 frequencies given in Table 10 are close to theirs for Fe_3 (the largest difference is 6 cm^{-1}) and Fe_4^+ (the largest difference is 26 cm^{-1}), for Fe_3^+, they differ with our values by as much as 106 cm^{-1}. Our computed asymmetric stretching frequency of Fe_3 is in good agreement with the value of 180 cm^{-1} reported by Nour et al.,[13] but as noted above, Moscovits and co-workers questioned this assignment. We note that for Ni_3, our computed[74] value differs from experiment[13] by 20 cm^{-1}, suggesting that the Fe_3 asymmetric frequency, if not 180 cm^{-1} as assigned by Nour et al., is probably close to this value.

TABLE 11: Comparison of Theoretical and Experimental Electron Affinities and Ionization Energies of Iron Clusters

	Fe_2	Fe_3	Fe_4	Fe_5	Fe_6
			EA_{ad}, eV		
BPW91	0.94	1.47	1.76	1.84	1.61
LSDA[a]	0.95	1.37	1.69	2.08	
PP86[b]	1.17	1.73	2.10		
Expl[c]	0.902(8)[d]	1.47(8)	1.72(8)	1.81(8)	1.51(8)
Expl[e]		1.43(6)	1.78(6)	1.84(6)	1.58(6)
			IE_{ad}, eV		
BPW91	6.68	5.82	5.71	6.04	6.15
LSDA[a]	7.21	6.27	5.90	6.37	
PP86[b]	7.14	6.28	6.20		
Expl[f]	6.30(1)	6.45(5)	6.4(1)	5.95(5)	5.9(1)
Expl[g]				6.20	5.96
Expl[h]			6.78(36)	6.30(12)	6.26(16)

[a] Ref 34. [b] Ref 47. [c] Ref 15. [d] Ref 12. [e] Ref 16. [f] Ref 17. [g] Ref 18. [h] Ref 19.

Electron Affinities and Ionization Energies. Computed adiabatic electron affinities (EA) and ionization energies (IE) are compared to experiment in Table 11. There is remarkably good agreement between the BPW91 EAs and most recent[16] experimental values obtained by laser photodetachment spectroscopy. The largest discrepancy is only 0.03 eV, which is within the experimental uncertainty of ±0.06 eV. Unexpectedly, the PP86 values differ from the experimental values to a larger extent than the LSDA values.

Laser photoionization has been used to determine the ionization thresholds, which probably correspond to vertical ionization energies (IEs). For Fe_2 and Fe_3, only one experimental study[17] appears to have been published. For Fe_4 to Fe_6, there are more than one experimental values, and they show differences with each other of up to almost 0.4 eV, see Table 11. Our values, which are presented in Table 11, are adiabatic values. However, our computed vertical IEs show only small differences (less than 0.1 eV) with the adiabatic values, except for Fe_4, where the vertical IE to the cation ground state with $2S + 1 = 12$

TABLE 12: Theoretical (BPW91) and Experimental Fragmentation Energies of Neutral and Charged Iron Clusters

neutral			anion		cation		
channel	TW	exp[a]	channel	TW	channel	TW	exp[a,b]
$Fe_2 \rightarrow Fe+Fe$	2.18	1.18	$Fe_2^- \rightarrow Fe^-+Fe$	2.53	$Fe_2^+ \rightarrow Fe^++Fe$	3.35	2.78
$Fe_3 \rightarrow Fe_2+Fe$	2.32	1.91	$Fe_3^- \rightarrow Fe_2+Fe^-$	3.18	$Fe_3^+ \rightarrow Fe_2^++Fe$	3.17	1.75
			$\rightarrow Fe_2^-+Fe$	3.84	$\rightarrow Fe_2+Fe^+$	4.34	3.20
$Fe_4 \rightarrow Fe_3+Fe$	3.06	2.19	$Fe_4^- \rightarrow Fe_3+Fe^-$	4.20	$Fe_4^+ \rightarrow Fe_3^++Fe$	3.13	2.28
$\rightarrow Fe_2+Fe_2$	3.13		$\rightarrow Fe_3^-+Fe$	3.34	$\rightarrow Fe_3+Fe^+$	5.14	
			$\rightarrow Fe_2+Fe_2^-$	4.00	$\rightarrow Fe_2+Fe_2^+$	4.11	2.50
$Fe_5 \rightarrow Fe_4+Fe$	3.26	2.25	$Fe_5^- \rightarrow Fe_4+Fe^-$	4.54	$Fe_5^+ \rightarrow Fe_4^++Fe$	3.00	2.69
$\rightarrow Fe_3+Fe_2$	4.17		$\rightarrow Fe_4^-+Fe$	3.37	$\rightarrow Fe_4+Fe^+$	5.10	
			$\rightarrow Fe_3+Fe_2^-$	5.04	$\rightarrow Fe_2+Fe_3^+$	3.91	3.40
			$\rightarrow Fe_3^-+Fe_2$	4.52	$\rightarrow Fe_2^++Fe_3$	4.79	3.20
$Fe_6 \rightarrow Fe_5+Fe$	3.74	3.17	$Fe_6^- \rightarrow Fe_5+Fe^-$	4.74	$Fe_6^+ \rightarrow Fe_5^++Fe$	3.57	3.26
$\rightarrow Fe_4+Fe_2$	4.86		$\rightarrow Fe_5^-+Fe$	3.51	$\rightarrow Fe_5+Fe^+$	5.36	
$\rightarrow Fe_3+Fe_3$	5.57		$\rightarrow Fe_4+Fe_2^-$	5.52	$\rightarrow Fe_4+Fe_2^+$	5.33	
			$\rightarrow Fe_4^-+Fe_2$	4.69	$\rightarrow Fe_4^++Fe_2$	4.38	
			$\rightarrow Fe_3+Fe_3^-$	5.71	$\rightarrow Fe_3+Fe_3^+$	5.18	

[a] Ref 25. For channels other than $Fe_n^+ \rightarrow Fe_{n-1}^++Fe$, the data are from ref 20.

(nonone-electron process) is 6.03 eV and to the cation state with $2S + 1 = 14$ is 6.21 eV. This latter value corresponds to a one-electron process and is much closer to the experiment. Our IEs for Fe_5 and Fe_6 are in good agreement with experiment. The largest (0.6 eV) discrepancy with experiment is found for the IE of Fe_3, assuming that the experimental IE for Fe_4 corresponds to the computed vertical one-electron process.

Local Magnetic Moments of the Neutral Clusters. The Fe_2 bonding pattern shows that there is a (4s + 4s) bonding orbital in each spin representation; the 3d spin-up electrons occupy localized atomic spin−orbitals and the 3d spin-down electrons occupy bonding orbitals. The local magnetic moments on atoms are defined by the difference in the number of their spin-up and spin-down electrons. Because the effective atomic 3d electronic configurations in the dimer are $3d^7$, the local magnetic moment on each Fe atom is $3\mu_B$.

The NBO analysis shows that the bonding patterns in larger iron Fe_n clusters have similarities to those in Fe_2, but also show some significant differences. For all systems, the Fe atomic occupation is essentially $4s^13d^7$. Thus, the 3d electrons contribute $3\mu_B$ at all atomic sites. In Fe_2, both 4s electrons are in a bonding (4s + 4s) orbital, and therefore do not contribute to the local magnetic moment. This is not true of the larger clusters, where some of 4s electrons occupy open-shell orbitals and therefore contribute to the local magnetic moment. We should note that "4s" orbitals actually show some mixing with the 3d orbitals and the NBO analysis shows that this hybridization increases from Fe_3 to Fe_6. While this mixing does not significantly affect the results for clusters containing up to six Fe atoms, it could become important for larger clusters.

In the $^{11}A_2$ ground state of Fe_3, the atomic occupation of the apex atom is $4s^{1.33}3d^{6.79}4p^{0.06}$, while those of the base atoms are $4s^{0.90}3d^{6.93}4p^{0.06}$. The three 4s electrons occupy one two-electron bond and one one-electron spin-up bond, thus the 4s electrons contribute to the local magnetic moment, which is now larger than found for Fe_2, namely $3.7\mu_B$ and $3.2\mu_B$ on the apex and basal atoms, respectively (see Figure 6).

All four atoms of ground-state Fe_4 have the same effective atomic occupation ($4s^{1.07}3d^{6.85}4p^{0.07}$). The four 4s electrons occupy one two-electron bond and two one-electron bonds and therefore contribute $2\mu_B$ to the total magnetic moment. Because the 4s electrons are evenly distributed on the Fe atoms, the local magnetic moments is $3.5\mu_B$ on each Fe atom. In Fe_5, the 4s electrons occupy two two-electron bonds and one one-electron bond, thus contributing $1\mu_B$ to the total magnetic moment. Due to its C_{2v} symmetry, Fe_5 possesses three types of atoms, see Figure 8. They have occupations and local magnetic moments of $4s^{0.60}3d^{7.04}4p^{0.09}$ and $2.9\mu_B$, $4s^{1.05}3d^{6.90}4p^{0.07}$ and $3.3\mu_B$, and $4s^{1.20}3d^{6.83}4p^{0.05}$ and $3.2\mu_B$. Clearly, the open-shell 4s electron is not evenly distributed among the Fe atoms.

In Fe_6, the apex and basal atoms have occupation of $4s^{1.03}3d^{6.94}4p^{0.08}$ and $4s^{1.03}3d^{6.86}4p^{0.06}$, respectively. With four spin-up and two spin-down 4s electrons, the 4s electrons contribute $2\mu_B$ to the total magnetic moment. Thus, the local magnetic moments of Fe_3 to Fe_6 are, on the average, larger than that found for Fe_2 due to contributions from the 4s electron. For Fe_4 and Fe_6, a spin pairing of the 4s electrons could have occurred which would have resulted in the same local magnetic moment as in Fe_2. Clearly, changes in the bonding must occur for larger clusters that to lead to a reduction in the local magnetic moment. Perhaps additional 4s to 3d promotion or 4s3d hybridization occurs, so that the "4s" one-electron bonds begin to appear in the spin down representation so that they reduce the magnetic moment rather than increase it.

Thermodynamic Stability. Fragmentation energies of positively charged iron clusters have been obtained[20] from collision induced-dissociation experiments, while the neutral cluster bond rupture energies (Fe_{n-1}−Fe) were estimated[25] from the cation CID data and the experimental IEs. The recommended[23,25] values of fragmentation energies are compared with our values computed at the BPW91 level in Table 12.

At the first glance, the theory overestimates the fragmentation energy by about 1 eV. It is known (see, e. g., ref 75) that the present DFT methods do not accurately describe the $^5D(4s^2-3d^6)$ ground state of Fe atom, but in fact yield an occupation that is a mixture of $4s^23d^6$ and $4s^13d^7$.This problem with the description of the Fe atom could be part of the reason for overestimating the bond rupture energies. For the neutral clusters, an additional source of error could be due to the differences in computed and experimental IEs, which have been used for deducing the bond rupture energies. Despite the overestimation of the bond energies, theory reproduces the experimentally observed trend of a general increase in the thermodynamic stability with increasing cluster size.

Conclusion

Our calculations on Fe_3, Fe_4, Fe_3^-, and Fe_4^- suggest that one should avoid using the LSDA, B3LYP, and BLYP approaches

when studying the structure of iron clusters. The Perdew family of correlation functionals provides similar structures and electronic properties. The use of the Becke or the Perdew-Burke-Ernzerhof exchange functionals yields essentially the same results as comparison of the BPBE or PBEPBE results show. The BPW91, BPBE, and PBEPBE approaches provide nearly the same values for the bond lengths, the vibrational frequencies, and the electron affinities. The latter are in remarkably good agreement with experiment. The BP86 level provides somewhat worse agreement with experiment. High local magnetic moments at iron sites are related to a specific type of chemical bonding in iron clusters. Effective atomic occupation is $(4s^{1+/-\delta}3d^{7-/+\delta})$ where δ is generally small. The 3d electrons contribute $3\mu_B$ per atom. The 4s electrons are not all paired in two-electron bonds, and therefore they also contribute to the magnetic moment. For the cluster sizes considered, we do not see a strong indication of a decreasing magnetic moment with cluster size. However, there is an increase in the 4s3d hybridization with cluster size, which leads us to speculate that as the cluster size increases, eventually either additional 4s to 3d promotion, or more likely, increased hybridization, will lead to an increase in the spin-down occupation at the expense of the spin-up occupation, resulting in a decrease in the local magnetic moment. In agreement with experiment, thermodynamic stability increases when moving from Fe_2 to Fe_6.

Acknowledgment. This work was supported by NASA Grant No. NCC2-5415 to the University of Virginia and from NASA Ames Research Center through contract NAS2-99092 to Eloret Corporation to G. L. G.

References and Notes

(1) Iijima, S.; Ichihashi, T. *Nature* **1993**, *363*, 603.
(2) Bethune, D. S.; Kiang, C. H.; deVries, M. S.; Gorman, G.; Savoy, R.; Vazquez, J.; Beers, R. *Nature* **1993**, *363*, 605.
(3) Nikolaev, P.; Bronikowski, M. J.; Bradley, R. K.; Rohmund, F.; Colbert, D. T.; Smith, K. A.; Smalley, R. E. *Chem. Phys. Lett.* **1999**, *313*, 91.
(4) Huisken, F.; Kohn, B.; Alexandrescu, R.; Morjan, I. *Eur. Phys. J. D* **1999**, *9*, 141.
(5) Delzeit, L.; McAninch, I.; Cruden, B. A.; Hash, D.; Chen, B.; Han, J.; Meyyappan, M. *J. Appl. Phys.* **2002**, *91*, 6027.
(6) Plönjes, E.; Palm, P.; Viswanathan, G. B.; Subramaniam, V. V.; Adamovich, I. V.; Lempert, W. R.; Fraser, H. L.; Rich, J. W. *Chem. Phys. Lett.* **2002**, *352*, 342.
(7) Dateo, C.; Gökçen. T.; Meyyappan, M. *J. Nanosci. Nanotech.* **2002**, *2*, 523.
(8) Dateo, C.; Gökçen. T.; Meyyappan, M. *J. Nanosci. Nanotech*. **2002**, *2*, 535.
(9) Montano, P. A. *Solid State Commun*. **1980**, *35*, 53.
(10) Purdum, H.; Montano, P. A.; Shenoy, G. K.; Morrison, T. *Phys. Rev. B* **1982**, *25*, 4412.
(11) Moskowits M.; DiLella, D. P. *J. Chem. Phys.* **1980**, *73*, 4917.
(12) Leopold, D. G.; Lineberger, W. C. *J. Chem. Phys*. **1986**, *85*, 51.
(13) Nour, E. M.; Alfaro-Franco, C.; Gingerich, K. A.; Laane, J. *J. Chem. Phys.* **1987**, *86*, 4779.
(14) Haslett, T. L.; Bosnick, K. A.; Fedrigo, S.; Moskowits M.; *J. Chem. Phys.* **1999**, *111*, 6456
(15) Wang. L. S.; Cheng, H. S.; Fan, J. *J. Chem. Phys*. **1995**, *102*, 9480.
(16) Wang. L. S.; Li, X.; Zhang, H. F. *Chem. Phys*. **2000**, *262*, 53.
(17) Rohlfing, E. A.; Cox, D. M.; Kaldor, A.; Johnson, K. H. *J. Chem. Phys*. **1984**, *81*, 3846.
(18) Yang, S.; Knickelbein, M. B. *J. Chem. Phys*. **1990**, *93*, 1533.
(19) Parks, E. K.; Klots, T. D.; Riley, S. J. *J. Chem. Phys*. **1990**, *92*, 3813.
(20) Brucat, P. J.; Zheng, L.-S.; Pettiette, C. L.; Yang, S.; Smalley, R. E. *J. Chem. Phys*. **1986**, *84*, 3078.
(21) Loh, S. K.; Hales, D. A.; Lian, L.; Armentrout, P. B. *J. Chem. Phys*. **1989**, *90*, 5466.
(22) Lian, L.; Su, C.-X.; Armentrout, P. B. *J. Chem. Phys*. **1992**, *97*, 4072.
(23) Armentrout, P. B. In *Metal−Ligand Interactions: Structure and Reactivity*; Vol. 474 of NATO Advanced Studies Institute, Science Series C: Mathematical and Physical Sciences; Russo, N., Salahub, D. R., Eds.; Kluwer Academic Publishers: Amsterdam, 1996; p 23.
(24) Markin, E. M.; Sugawara, K. *J. Phys. Chem. A* **2000**, *104*, 1416.
(25) Armentrout, P. B. *Annu. Rev. Phys. Chem*. **2001**, *52*, 423−61.
(26) Châtelain, A. *Philos. Mag. B* **1999**, *79*, 1367. Hirt, A.; Gerion, D.; Billas, I. M. L.; Châtelain, A.; de Heer, W. A. *Z. Phys. D* **1997**, *40*, 160.
(27) Billas, I. M. L.; Châtelain, A.; de Heer, W. A. *Science* **1994**, *265*, 1682.
(28) Cox, D. M.; Trevor, D. J.; Whetten, R. L.; Rohlfing, E. A.; Kaldor, A. *Phys. Rev. B* **1985**, *32*, 7290.
(29) Morse, M. D. *Chem. Rev*. **1986**, *86*, 1049. Salahub, D. R. In *Ab Initio Methods in Quantum Chemistry − II*, Lawley, K. P., Ed.; Wiley: New York, 1987; pp 447—520; Dhar, S.; Kestner, N. R. *Phys. Rev. A* **1988**, *38*, 1111. Tomonari, M.; Tatewaki, H. *J. Chem. Phys*. **1988**, *88*, 1828. Pavão, A. C.; Taft, C. A.; Hammond, B. L.; Lester, W. A., Jr. *Phys. Rev. B* **1989**, *40*, 2879. Noro, T.; Ballard, C.; Palmer, M. H.; Tatewaki, H. *J. Chem. Phys*. **1994**, *100*, 452. Yanasigava, S.; Tsuneda, T.; Hirao, K. *J. Chem. Phys*. **2000**, *112*, 545. Barden, C. J.; Rienstra-Kiracofe, J. C.; Schaefer, H. F., III *J. Chem. Phys*. **2000**, *113*, 690.
(30) Tatewaki, H.; Tomonari, M.; Nakamura, T. *J. Chem. Phys*. **1988**, *88*, 6419.
(31) Dunlap, B. I. *Phys. Rev. A* **1990**, *41*, 5691.
(32) Chen, J. L.; Wang, C. S.; Jackson, K. A.; Pederson, M. R. *Phys. Rev. B* **1991**, *44*, 6558.
(33) Cheng, H.-P.; Ellis, D. E. *J. Chem. Phys*. **1991**, *94*, 3735.
(34) Castro, M.; Salahub, D. R. *Phys. Rev. B* **1994**, *49*, 11842.
(35) Gong, X. G.; Zheng, Q. Q. *J. Phys. Condens. Matter* **1995**, *7*, 2421.
(36) Ballone, P.; Jones, R. O. *Chem. Phys. Lett.* **1995**, *233*, 632,
(37) Castro, M. *Int. J. Quantum Chem*. **1997**, *64*, 223.
(38) Oda, T.; Pasquarello, A.; Car, R. *Phys. Rev. Lett*. **1998**, *80*, 3622.
(39) Castro, M.; Jamorski, K.; Salahub, D. R. *Chem. Phys. Lett.* **1997**, *271*, 133.
(40) Gutsev, G. L.; Khanna, S. N.; Jena, P. *Phys. Rev. B* **2000**, *62*, 1604.
(41) Diéguez, O.; Alemany, M. M. G.; Rey, C.; Ordejón, P.; Gallego, L. J. *Phys. Rev. B* **2001**, *63*, 205407.
(42) Gutsev, G. L. *Phys. Rev. B* **2002**, *65*, 132417.
(43) Bobadova-Parvanova, P.; Jackson, K. A.; Srinivas, S.; Horoi, M.; Köhler, C.; Seifert, G. *J. Chem. Phys*. **2002**, *116*, 3576.
(44) Christensen, O. B.; Cohen, M. L. *Phys. Rev. B* **1993**, *47*, 13643.
(45) Andriotis, A. N.; Menon, M. *Phys. Rev. B* **1998**, *57*, 10069.
(46) Duan, H. M.; Zheng, Q. Q. *Phys. Lett. A* **2001**, *280*, 333.
(47) Chrétien, S.; Salahub, D. R. *Phys. Rev. B* **2002**, *66*, 155425.
(48) Kohn, W.; Sham, L. J. *Phys. Rev. A* **1965**, *140*, 1133.
(49) Becke, A. D. *Phys. Rev. A* **1988**, *38*, 3098.
(50) Perdew, J. P.; Wang, Y. *Phys. Rev. B* **1992**, *45*, 13244.
(51) Slater, J. C. *Quantum Theory of Molecular and Solids.* Vol. 4: *The Self-Consistent Field for Molecular and Solids*; McGraw-Hill: New York, 1974.
(52) Vosko, S. H.; Wilk, L.; Nusair, M. *Can. J. Phys*. **1980**, *58*, 1200.
(53) Becke, A. D. *J. Chem. Phys.* **1993**, *98*, 5648.
(54) Stevens, P. J.; Devlin, F. J.; Chablowski, C. F.; Frisch, M. J. *J. Phys. Chem.* **1994**, *98*, 11623.
(55) Lee, C.; Yang, W.; Parr, R. G. *Phys. Rev. B* **1988**, *37*, 785.
(56) Perdew, J. P. *Phys. Rev. B* **1986**, *33*, 8822.
(57) Perdew, J. P.; Burke, K.; Ernzerhof, M. *Phys. Rev. Lett.* **1996**, *77*, 3865.
(58) Frisch, M. J.; Trucks, G. W.; Schlegel, H. B.; Scuseria, G. E.; Robb, M. A.; Cheeseman, J. R.; Zakrzewski, V. G.; Montgomery, J. A., Jr.; Stratmann, R. E.; Burant, J. C.; Dapprich, S.; Millam, J. M.; Daniels, A. D.; Kudin, K. N.; Strain, M. C.; Farkas, O.; Tomasi, J.; Barone, V.; Cossi, M.; Cammi, R.; Mennucci, B.; Pomelli, C.; Adamo, C.; Clifford, S.; Ochterski, J.; Petersson, G. A.; Ayala, P. Y.; Cui, Q.; Morokuma, K.; Malick, D. K.; Rabuck, A. D.; Raghavachari, K.; Foresman, J. B.; Cioslowski, J.; Ortiz, J. V.; Stefanov, B. B.; Liu, G.; Liashenko, A.; Piskorz, P.; Komaromi, I.; Gomperts, R.; Martin, R. L.; Fox, D. J.; Keith, T.; Al-Laham, M. A.; Peng, C. Y.; Nanayakkara, A.; Gonzalez, C.; Challacombe, M.; Gill, P. M. W.; Johnson, B. G.; Chen, W.; Wong, M. W.; Andres, J. L.; Head-Gordon, M.; Replogle, E. S.; Pople, J. A. *Gaussian 98*, revision A.11; Gaussian, Inc.: Pittsburgh, PA, 1998.
(59) Wachters, A. J. H. *J. Chem. Phys.* **1970**, *52*, 1033.
(60) Hay, P. J. *J. Chem. Phys.* **1977**, *66*, 4377.
(61) Raghavachari, K.; Trucks, G. W. *J. Chem. Phys.* **1989**, *91*, 1062.
(62) Gutsev, G. L.; Bauschlicher, C. W., Jr. *J. Phys. Chem.* **2003**, *197*, 4755.
(63) Ricca, A.; Bauschlicher, C. W., Jr. *Theor. Chem. Acc.* **2001**, *106*, 314.
(64) Reed, A. E.; Weinstock, R. B.; Weinhold, F. *J. Chem. Phys*. **1985**, *83*, 735.
(65) Reed, A. E.; Curtiss, L. A.; Weinhold, F. *Chem. Rev*. **1988**, *88*, 899.
(66) Hübner, O.; Sauer, J. *Chem. Phys. Lett*. **2002**, *358*, 442.

(67) Bauschlicher, C. W., Jr.; Ricca, A. *Mol. Phys.* **2002**, *101*, 93.
(68) Gutsev, G. L.; Khanna, S. N.; Jena, P. *Chem. Phys. Lett.* **2001**, *345*, 481.
(69) Gutsev, G. L.; Bauschlicher, C. W., Jr.; Andrews, L. Structure and chemical bonding of 3d-metal anions. In *Theoretical Prospects of Negative Ions*;. Kalcher, J., Ed.; Research Signpost: Trivandrum, India, 2002; p 43−60.
(70) Morse, M. D. In *Advances in Metal and Semiconductor Clusters*; JAI Press Inc.: Greenwich, CT, 1993; Vol. 1, pp 83−121.
(71) Tremblay, B.; Manceron, L.; Gutsev, G. L.; Andrews, L. *J. Phys. Chem. A* **2002**, *106*, 10525.
(72) Tremblay, B.; Manceron, L.; Gutsev, G. L.; Andrews, L.; Partridge, H., III *J. Chem. Phys.* **2002**, *117*, 8479.
(73) Martin, J. M. L.; Bauschlicher, C. W., Jr.; Ricca, A. *Comput. Phys. Commun.* **2001**, *133*, 189.
(74) Gutsev, G. L.; Bauschlicher, C. W., Jr., to be published.
(75) Gutsev, G. L.; Bauschlicher, C. W., Jr., *Theor. Chem. Acc.* **2002**, *106*, 27.